Model-Independent Simulation Complexity of Complex Quantum Dynamics

Aiman Khan,[1,*] David Quigley,[1] Max Marcus[ ],[2] Erling Thyrhaug[ ],[3] and Animesh Datta[1,†]

[1]*Department of Physics, University of Warwick, Coventry CV4 7AL, United Kingdom*
[2]*Physical & Theoretical Chemistry Laboratory, Department of Chemistry, University of Oxford, Oxford OX1 3QZ, United Kingdom*
[3]*Dynamical Spectroscopy, Department of Chemistry, Technical University of Munich, 85748 Garching, Germany*

We present a model-independent measure of dynamical complexity based on simulation of complex quantum dynamics using stroboscopic Markovian dynamics. Tools from classical signal processing enable us to infer the Hilbert space dimension of the complex quantum system evolving under a time-independent Hamiltonian via pulsed interrogation. We illustrate this using simulated third-order pump-probe spectroscopy data for exciton transport in a toy model of a coupled dimer with vibrational levels, revealing the dimension of the singly excited manifold of the dimer. Finally, we probe the complexity of excitonic transport in light harvesting 2 (LH2) and Fenna-Matthews-Olson (FMO) complexes using data from two recent nonlinear ultrafast optical spectroscopy experiments. For the latter we make model-independent inferences that are commensurate with model-specific ones, including the estimation of the fewest number of parameters needed to fit the experimental data and identifying the spatial extent, i.e., delocalization size, of quantum states participating in this complex quantum dynamics.

Some of the most challenging yet exciting entities at the vanguard of our understanding in the physical sciences are complex quantum systems, ranging from molecular processes on the femtosecond timescale, such as many-body coherent dynamics in semiconductors [1], exciton transport processes in photosynthetic light harvesting complexes [2], ultrafast isomerization in rhodopsin which is the primary photochemical event in vision [3], to various processes in atomic, molecular, condensed matter, chemical, laser, and nuclear physics [4]. The "complexity" of any quantum dynamics must depend on the dimension of the Hilbert space which the process explores. Identifying this dimension is precisely the challenge since typical complex quantum systems involve an extended environment coupled to a finite-dimensional central core—such as vibrational levels interacting with excitons in light-harvesting complexes, resulting in, in principle, an infinite-dimensional Hilbert space. In practice, however, complex quantum dynamics often explore a small part of the environment around the central core resulting in an effective finite-dimensional Hilbert space. It is this that we seek to identify in this work.

The term "simulation complexity" was introduced in a model-dependent approach that used one-dimensional tensor networks to approximate the system-environment joint state [5]. The bond dimension of these networks was interpreted as the square of the effective environment dimension that can simulate open system dynamics. In another recent work, a fluctuation-dissipation theorem for chaotic systems at high temperatures was established, linking the time-averaged fluctuation of a probe observable to the average decay rate of the test qubit by a factor that depends on the effective Hilbert space dimension of the system and environment [6].

It has been shown that the dimensionality of the effective system-environment quantum state can be bounded in a model-independent way using tools from the theory of classical dynamical systems and signal processing on time series of experimental data [7–11]. This method of delays, as it is often called, computes the size of a fictitious, extended *quantum* system evolving under a fixed Markovian map that reproduces the given dynamics. We refer to this dimension-based classification of dynamical complexity as model-independent simulation complexity (MISC).

Similar to the method of delays, the reproduction of dynamics in a model-independent manner using a fixed Markovian map in the generalized probabilistic framework has also been achieved via other tools of subspace identification [12]. These methods have provided model-independent characterizations of the Hilbert space dimension of up to three engineered qubits [8,9,12]. Unfortunately, MISC based on the method of delays (or other subspace identification techniques) as developed in previous works cannot be applied directly to large families of experimental scenarios without accounting for and filtering out the transient effects of the time-dependent interactions. Prominent among them are linear and nonlinear spectroscopies where finite time-dependent interactions between pulses and the complex quantum systems are used to probe complex dynamics.

In this work, we develop MISC for use on time-integrated data generated from finite time-dependent

interactions. This allows us to overcome the transient effects of the time-dependent pulses. Next, we define, in a model-independent manner, MISC for noisy signals with signal-to-noise ratio bounded by ϵ (referred to as MISC_ϵ). Finally, we evaluate MISC_ϵ for simulated and experimental ultrafast nonlinear spectroscopy data from exciton transport in coupled dimers, and the light harvesting 2 (LH2) and Fenna-Matthews-Olson (FMO) complex, respectively. For the latter complex quantum dynamics, we make some model-independent inferences that are commensurate with model-specific inferences and electronic structure calculations. This suggest a role for MISC_ϵ in understanding challenging complex quantum systems.

Quantum system interrogated by pulses.—Suppose the Hamiltonian governing the quantum system is

$$\hat{H}(t) = \hat{H}_0 + \hat{V}(t), \tag{1}$$

where $\hat{V}(t) = \eta\hat{V}\sum_{k=1}^{N} g(t - T_k)$, η being the strength of system-pulse coupling, $g(t)$ is the pulse envelope, $\boldsymbol{T} = \{T_1, \ldots, T_N\}$ is the set of central times of the N pulses, and $\hat{V}$ is the interaction operator. $\hat{H}(t)$ encompasses, among other experimental scenarios, linear and nonlinear spectroscopy of complex quantum systems. In all these cases, the time-integrated signal is

$$E(\boldsymbol{T}) = \int_{-\infty}^{\infty} dt_I \langle \psi(t)|\hat{V}_I(t)|\psi(t)\rangle_I, \tag{2}$$

where $|\psi(t)\rangle_I = e^{i\hat{H}_0 t}|\psi(t)\rangle$, $\hat{V}_I(t) = e^{i\hat{H}_0 t}\hat{V}e^{-i\hat{H}_0 t}$ are the interaction-picture state and evolution operator, respectively.

Assuming the pulses do not overlap (the semi-impulsive limit), $g(t - T_k)g(t - T_l) = 0 \; \forall \; T_k \neq T_l \in \boldsymbol{T}$, and the interaction operator and system Hamiltonian do not commute $[\hat{H}_0, \hat{V}] \neq 0$, the time-integrated signal is (see Supplemental Material [13], Sec. A)

$$E(\boldsymbol{T}) = i\hbar \sum_{k,l=0}^{\infty} \sum_{m=0}^{k} E_{k-m,l+m+1}(\boldsymbol{T}), \tag{3}$$

where $E_{kl}(\boldsymbol{T}) = {}_I\langle\psi^k(\infty)||\psi^l(\infty)\rangle_I$ is the overlap of the interaction-picture asymptotic wave functions, defined as $|\psi^{(n)}(t)\rangle_I = \hat{U}_n(t, t_0)|\psi_0\rangle$, where

$$\hat{U}_I(t, t_0) = \sum_{m=0}^{\infty} \hat{U}_n(t, t_0),$$

$$\hat{U}_n(t, t_0) = \left(-\frac{i}{\hbar}\right)^n \int_{t_0}^{t} dt_1 \ldots \int_{t_0}^{t_{n-1}} dt_n \hat{V}_I(t_1)\ldots\hat{V}_I(t_n). \tag{4}$$

To simplify the subsequent exposition, we focus on the signal as the function of a single time difference $\delta T_\alpha = T_{\alpha+1} - T_\alpha$, in which case each term in Eq. (3) is of the form (see Supplemental Material [13], Sec. A)

$$E_{kl}(\delta T_\alpha) = \sum_{\lambda} c_{kl}(\lambda)\chi_{abcd}(\delta T_\alpha) + \text{const}, \tag{5}$$

$\lambda = \{\lambda_a, \lambda_b, \lambda_c, \lambda_d\}$ is a quadruplet of indices, each indexing a complete set of basis vectors $\sum_a |\lambda_a\rangle\langle\lambda_a| = I$ and so on, and $\chi_{abcd}(t) = \langle\lambda_a|e^{i\hat{H}_0 t}|\lambda_b\rangle\langle\lambda_c|e^{-i\hat{H}_0 t}|\lambda_d\rangle$ are process tensor elements corresponding to unitary evolution effected by Hamiltonian $\hat{H}_0$. The coefficients $c_{kl}(\lambda)$ are defined in Supplemental Material [13], Sec. A.

Using Eqs. (3) and (5), the time-integrated signal is, up to an additive constant,

$$E(\delta T_\alpha) = i\hbar \sum_{k,l=0}^{\infty} \sum_{m=0}^{k} \sum_{\lambda} c_{k-m,l+m+1}(\lambda)\chi_{abcd}(\delta T_\alpha), \tag{6}$$

a linear combination of process tensor elements that evolve via the time-independent Hamiltonian $\hat{H}_0$ only. Importantly, this form allows us to sidestep the additional complexity imposed by transient effects of the time-dependent interaction Hamiltonian $\hat{V}(t)$ and instead capture the complexity of quantum dynamics induced by $\hat{H}_0$ only. The form of the signal in Eq. (6) is now ready for discrete time series analysis using the method of delays to bound the complexity of quantum dynamics. This method of delays can also be applied directly to transient time series of expectation values—however, this can lead to identification of spuriously high complexity, as discussed in detail in Supplemental Material [13], Sec. B.

Method of delays: Consider a finite stream of data $\boldsymbol{A} \equiv A(k) \in \mathbb{R}, k \in \mathbb{N}_K \equiv \{0, 1, \ldots, K\}$, recorded as a discrete function of a relevant dynamical control variable indexed by k, typically time. This encompasses $E(\delta T_\alpha)$ discussed previously (where the dynamical control variable would be the time delay between successive pulses). A numerical value of MISC can be extracted from the data by invoking two related results from the method of delays in quantum information theory [7–9]. First, given a discrete bounded time series, there always exist an initial quantum state $\hat{\rho}_0$, a fixed generator $\mathcal{P}$ of stroboscopic Markovian dynamics [8,14–17], and quantum observable $\hat{A}$ acting on Hilbert space of dimension $\text{rank}(M) + 2$ where

$$M_{mn} = A(m + n - 2); \qquad m, n \in \{1, \ldots, K\}, \tag{7}$$

such that $A(k) = \text{Tr}(\hat{A}\mathcal{P}^k\rho_0) \; \forall \; k \in \mathbb{N}_K$. The $\lceil K/2 \rceil \times \lceil K/2 \rceil$-sized square matrix M is referred to as the time delay (TD) matrix, giving the eponymous method [7]. Second, if the evolution of a given quantum state is in fact known beforehand to be given by the stroboscopic Markovian map generated by $\mathcal{Q}$ [so that $A(k) = \text{Tr}[\hat{A}\mathcal{Q}^k\hat{\rho}_0]$], the inequality $\sqrt{\text{rank}(M)} \leq d$ holds, where d is the Hilbert space dimension of relevant dynamics. Combining both results [7], for *arbitrary* dynamics,

$$\sqrt{\text{rank}(M)} \leq d \leq \text{rank}(M) + 2, \qquad (8)$$

where d is interpreted as the dimension of the smallest quantum system that can simulate the complex, possibly non-Markovian, quantum dynamics using homogeneous, stroboscopic Markovian dynamics. As both the upper and lower bounds of d are model-independent functions of the rank of the delay matrix, we define

$$\text{MISC} = \sqrt{\text{rank}(M)} \qquad (9)$$

as the model-independent simulation complexity (MISC). The method of delays can be further used to explicitly construct simulated quantum (or otherwise) realizations of open system dynamics [9–11], which we do not discuss any further because our interest here lies in the evaluation of simulation complexity only.

For the TD matrix M^E obtained from signal $E(\delta T_\alpha)$ in Eq. (6), a tighter bound corresponding to unitary evolutions [8]

$$\text{rank}(M^E) \leq d_0^2 + d_0 - 1, \qquad (10)$$

follows, where d_0 is the dimension of the subspace of $\hat{H}_0$ on which $\hat{V}$ acts.

MISC with relative error.—In practice, $A(k)$ (or indeed any signal), is inevitably contaminated by noise. This affects the computation of MISC as a TD matrix M constructed from a noisy $A(k)$, irrespective of the length or resolution of the time series, tends to have full rank. Instead, we evaluate the numerical rank of M which requires, first and foremost, a meaningful delineation of the singular value spectrum of M into noisy and non-noisy components. The singular value spectrum is defined by the decomposition $M = \sum_{i=1}^{\lceil K/2 \rceil} O_1 \Sigma_i O_2$, where $O_{1,2}$ are orthogonal matrices and Σ_i are the singular values in descending order. In order to evaluate numerical rank, the singular values attributed to noise are set to zero [18].

To this end, consider the reconstructed signal time series A_r formed from the TD matrix $M_r = \sum_{i=1}^{r} O_1 \Sigma_i O_2$, and define the root mean square perturbation as

$$\Delta_r = \frac{\|A_r - A\|_2}{\|A\|_2}, \qquad (11)$$

where $\| \cdot \|_2$ is the 2-norm, defined as $\|A\|_2 = \sqrt{\sum_{k=0}^{K} |A(k)|^2}$. Starting with the intuition that noise will only contribute to small values in the singular value spectrum [20] of the delay matrix M, we define the MISC with relative error ϵ as

$$\text{MISC}_\epsilon = \sqrt{R}, \quad \text{where } R = r : \Delta_r < \epsilon < \Delta_{r-1} \qquad (12)$$

for $r \in \{1, ..., \lceil K/2 \rceil\}$. Here, ϵ captures the relative error with which the dynamics captured by the discrete time

series $A(k)$ are reproduced by the stroboscopic Markovian simulator. The choice of ϵ is determined by the signal-to-noise ratio (SNR) in $A(k)$ which sets the meaningful precision to which it is reproduced. For numerical simulations, ϵ is proportional to the precision of the numerical solver employed, whereas for experimental data it is inversely proportional to its SNR.

An important consideration in the evaluation of MISC_ϵ is its dependence on the length and resolution of the time series—K data points can reveal a maximum simulation complexity of $\sqrt{\lceil K/2 \rceil}$, and excessive coarse graining of observations progressively reduces the computed MISC_ϵ. Depending on the complex quantum system at hand there may be an insufficient amount of data, which may pose a challenge in certain experiments [8]. This is indeed revealed in a single-molecule spectroscopy experiment we analyze in a later section. It is possible to use the Nyquist sampling theorem (which dictates that the minimum sampling rate that fully reconstructs a finite-bandwidth continuous signal is twice its highest frequency component) may be used to estimate the appropriate sampling rate needed to evaluate a meaningful MISC_ϵ. However, for simulated data in the following sections, we evaluate MISC_ϵ by directly checking for its stability against changes in duration and sampling rate of the signal.

As expected of any reasonable measure of simulation complexity, MISC_ϵ also depends on the tolerance up to which we seek to reproduce the complex quantum system dynamics. As is also expected, Eq. (12) shows that *ceteris paribus*, MISC_ϵ is a monotonically decreasing function of ϵ. This is illustrated for the Jaynes-Cummings model in Fig. C.2, discussed in Supplemental Material [13], Sec. C. We also evaluate MISC_ϵ for population and coherence dynamics in the spin boson model (Supplemental Material [13], Sec. E), a bona fide open system governed by time-independent Hamiltonian dynamics.

MISC_ϵ for simulated and experimental nonlinear spectroscopy data.—We now evaluate the model-independent simulation complexity with relative error ϵ—MISC_ϵ—for excitonic transport in photosynthetic light harvesting complexes [2]. These dynamics are driven by strong exciton-phonon interactions which render them complex quantum systems, and are most fruitfully studied using ultrafast nonlinear spectroscopy [2,21–25] for which the recorded signal is of the form obtained in Eq. (6). Therefore, MISC_ϵ for these complex systems can be obtained precisely as for the open systems studied in Supplemental Material [13], Secs. C and E, except that the TD matrices are constructed using the time-integrated signal $E(\delta T_\alpha)$ recorded as a function of δT_α and that the tighter lower bound of Eq. (10) holds.

Simulated pump-probe spectroscopy of coupled dimer.—The strong exciton-phonon interaction in photosynthetic light harvesting complexes is often modeled using the Frenkel-Holstein Hamiltonian $\hat{H}_{\text{FH}} = \hat{H}_{\text{exc}} + \hat{H}_{\text{ph}} + \hat{H}_{\text{exc-ph}}$

where the successive terms denote the exciton, phonon, and interaction Hamiltonians. For a dimer

$$\hat{H}_{\mathrm{exc}} = \sum_{i=1,2} \varepsilon_i \hat{c}_i^\dagger \hat{c}_i + \kappa(\hat{c}_1^\dagger \hat{c}_2 + \hat{c}_1^\dagger \hat{c}_2), \qquad (13)$$

$$\hat{H}_{\mathrm{ph}} = \sum_{i=1,2} \hbar\omega_i(\hat{d}_i^\dagger \hat{d}_i + 1/2), \qquad (14)$$

$$\hat{H}_{\mathrm{exc\text{-}ph}} = -\sum_{i=1,2} \hbar\omega_i g_i \hat{c}_i^\dagger \hat{c}_i(\hat{d}_i^\dagger + \hat{d}_i), \qquad (15)$$

where ε_i are the on-site energies, κ is the strength of dipole-dipole coupling between the sites 1 and 2, $\{\hat{c}_i^\dagger, \hat{c}_i\}$ are the creation-annihilation operator pair for the two sites, $\{\hat{d}_i^\dagger, \hat{d}_i\}$ are the phonon creation-annihilation operator pair for vibrational bath coupled to each site, ω_i are the phonon frequencies for the vibrational ladders, and g_i are the individual strengths of the phonon-exciton coupling.

Table I displays the MISC_ϵ evaluated using the simulated signal generated from a sequence of four distinct pump-probe experiments [26] used to investigate singly excited manifold (SEM) dynamics of the dimer, for a varying number of phonons in the vibrational bath (See Supplemental Material [13], Sec. G for details). Each component signal is aggregated over 300 molecules with varying dipole orientations corresponding to individual sites but fixed relative orientation of 40°. In order to simultaneously take into account the four distinct signals that are recorded, we construct TD tensors (in place of TD matrices) whose spanned space will be bound by the same inequality as Eq. (8). The simulation complexity is then set to be the maximum of MISC_ϵ corresponding to all possible combinations of the signal components. As this is a simulation, the precise dimension of the complex quantum system's Hilbert space is known. MISC_ϵ is expectedly found to be always less than the Hilbert space dimension of the dimer SEM which is probed by the pump-probe experiment as presented in Table I. Furthermore, lower values of ϵ lead to larger complexity.

TABLE I. MISC_ϵ for $\epsilon = 10^{-1}$ and 10^{-4} calculated from TD tensors constructed out of aggregate signals corresponding to 2800 time delays, chosen uniformly between 0.5 and 6.098 ps for pump-probe spectroscopy of dimer molecules. The dimer parameters are taken to be those of the allophycocyanin (APC) molecule (See Supplemental Material [13], Sec. G).

No. of Phonons	$\mathrm{MISC}_{\epsilon=10^{-1}}$	$\mathrm{MISC}_{\epsilon=10^{-4}}$	SEM dimension
0	1.41	1.73	2
1	1.73	3.74	4
2	2.82	6.40	9
3	8.48	13.30	16
4	11.74	21.61	25

Experimental single-molecule pump-probe spectroscopy of the LH2 complex.—We evaluate MISC_ϵ for excitonic transport in LH2 complexes using experimental data resulting from the excitation of single LH2 molecules with two phase-coherent ultrafast pulses [21]. The experiment was designed to explore quantum coherent population transfer over varying pathways in LH2 complexes. The time series, constructed from 17 data points, yields a full-rank TD matrix for $\epsilon = 10^{-1}$, meaning $\mathrm{MISC}_{\epsilon=10^{-1}} = 3.0$. This suggests that more data points are required to meaningfully quantify the simulation complexity of excitonic pathways in LH2 complexes.

Experimental 2D electronic spectroscopy of FMO complex.—Finally, we evaluate MISC_ϵ for excitonic transport in the FMO complex using experimental data from polarization-controlled 2D electronic spectroscopy [22]. The original experiment uses two distinct configurations of polarizations of the pulses—a sequence of four all-parallel (AP) pulses ($\langle 0°, 0°, 0°, 0°\rangle$) and the double-crossed (DC) sequences of pulses ($\langle 45°, -45°, 90°, 0°\rangle$). The experiment is designed to study both the short-lived excitonic coherence as well as the long-lived vibronic coherence of FMO dynamics at 77 K, recorded over several picoseconds. The spectra is generated as a sequence (for different population times t_2) of 2D plots of the complex emitted field, as a function of the excitation and detection energies (denoted by the wave numbers ν_1 and ν_3 here). The real and imaginary components of the emitted field are used to construct the time series and the evaluated MISC_ϵ are presented in Fig. 1.

Some observations are in order. First, the choice of different ϵ for the AP and DC data is motivated by the different SNRs in the two experiments. DC experiments
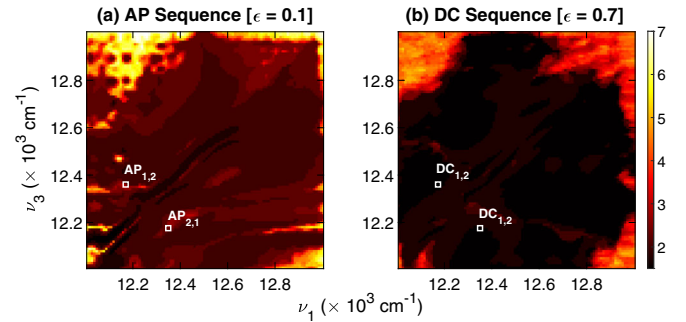

FIG. 1. Heat maps of MISC_ϵ for (a) AP ($\epsilon = 0.1$) and (b) DC ($\epsilon = 0.7$) pulse sequences for excitonic transport in the FMO complex using experimental data from polarization-controlled 2D electronic spectroscopy [22]. Each map is composed of a 100×100 grid of (ν_1, ν_3) points. Each point is generated from the time series of the complete rephasing signal $\tilde{E}^{(3)}(\nu_1, t_2, \nu_3)$, where ν_1 and ν_3 are proportional to the excitation and detection energies, and the complex emitted signal field is recorded (a) over 2.4 ps for the AP sequences, and (b) over 2.9 ps for DC sequences, each sampled every 20 fs. The cross peaks for both pulse sequences are marked with white boxes on the map.

have lower noise [27], but also detect smaller signals resulting in a lower SNR compared to the AP experiments. Indeed, MISC_ϵ for varying ϵ for the DC pulse sequence helps reveal the noise floor in the data, providing ϵ its physical interpretation (See Supplemental Material [13], Sec. H). Second, the AP MISC_ϵ map has a diagonal valley of low simulation complexity which subsumes the vicinities of the cross peaks linking the two lowest energy excitons, where particularly prominent oscillations were noted in the original study [22], specifically the $\text{AP}_{2,1}$ peak that corresponds exclusively to ground state vibrations. Third, the AP data reveal slightly higher complexity than the DC data as shown by the former's lighter shade. This is commensurate with the design of the DC experiment that suppresses some of the Liouville pathways present in the AP data to reveal certain weaker ones. Finally, a MISC_ϵ of 2 across most of the DC map shows that the intermolecular excitonic coherence effectively explores a two-dimensional Hilbert space, while the intramolecular vibrational motion that dominates the AP data involves no more than 3 Hilbert space dimensions. In conjunction with the fact that the FMO is constituted of identical bacteriochlorophyll a molecules, this suggests that the excitonic dynamics is fairly localized spatially, in qualitative agreement with electronic structure calculations [28].

The evaluated simulation complexity, rounded off to $\lceil \text{MISC}_\epsilon \rceil$, corresponds to the dimension of the smallest quantum system that can possibly reproduce measured dynamics of complex systems with relative error ϵ. This allows us to estimate the fewest number of parameters needed to reproduce the measured signal. To describe unambiguously stroboscopic Markovian dynamics on a Hilbert space of dimension d, one would require $3d^2 + d - 3$ real parameters to define the initial quantum state, the map generating stroboscopic Markovian dynamics as well the Hermitian observable whose expectation is used to reproduce the signal time series. Using the computed $\lceil \text{MISC}_\epsilon \rceil$ for the cross peaks [which is 3 for both the AP cross peaks in Fig. 1(a) and DC cross peaks in Fig. 1(b)], our framework predicts a minimum of 27 real parameters are required for both cross peaks of the AP and DC sequences. This compares with 24 parameters for AP cross peaks and 20 parameters for DC cross peaks used in the original study [22].

Conclusions and discussion.—We have developed a model-independent framework to quantify the dynamical complexity of quantum systems via MISC_ϵ that can be applied directly to experimental data stemming from experiments performed on complex systems. The model independence offers unambiguous interpretation in terms of the minimum number of parameters needed to simulate these experimental data using stroboscopic Markovian dynamics up to a desired relative error ϵ. We have illustrated this through numerically generated data from simple theoretical models as well as experimental data from nonlinear spectroscopy experiments of complex biological molecules.

The general nature of the MISC framework means that it can potentially be applied to diverse physical system beyond light harvesting complexes such as spectroscopic investigations of exciton dynamics in molecules, polymers, semiconductors, and ion chains using both classical and quantum light. The MISC_ϵ dimension inferred independently of any model can serve as the first quantity in understanding complex quantum systems. It can also be used to develop more elaborate models or compared to those from other, model-dependent recipes [5,6] to adjudicate the latter's viability. The full potential of our work can hence only be realized by applying it to data from future experiments on complex systems. A particularly relevant instance is determining the extent of certain complex quantum dynamics in physical space. As many of these systems, such as pigment-protein complexes, are constituted of simple molecular units, the Hilbert space dimension can provide an estimate of the number of units, and thus the spatial extent of the eigenstates participating in particular dynamics, aiding complicated electronic structure calculations [28,29].

[*]aiman.khan@warwick.ac.uk
[†]animesh.datta@warwick.ac.uk

[1] C. L. Smallwood and S. T. Cundiff, Multidimensional coherent spectroscopy of semiconductors, Laser Photonics Rev. **12**, 1800171 (2018).

[2] A. Chenu and G. D. Scholes, Coherence in energy transfer and photosynthesis, Annu. Rev. Phys. Chem. **66**, 69 (2015).

[3] D. Polli, P. Altoè, O. Weingart, K. M. Spillane, C. Manzoni, D. Brida, G. Tomasello, G. Orlandi, P. Kukura, R. A. Mathies, M. Garavelli, and G. Cerullo, Conical intersection dynamics of the primary photoisomerization event in vision, Nature (London) **467**, 440 (2010).

[4] V. M. Akulin, *Dynamics of Complex Quantum Systems* (Springer, Dordrecht, 2014).

[5] I. A. Luchnikov, S. V. Vintskevich, H. Ouerdane, and S. N. Filippov, Simulation Complexity of Open Quantum Dynamics: Connection with Tensor Networks, Phys. Rev. Lett. **122**, 160401 (2019).

[6] C. Nation and D. Porras, Ergodicity probes: Using time-fluctuations to measure the Hilbert space dimension, Quantum **3**, 207 (2019).

[7] M. M. Wolf and D. Perez-Garcia, Assessing Quantum Dimensionality from Observable Dynamics, Phys. Rev. Lett. **102**, 190504 (2009).

[8] A. Strikis, A. Datta, and G. C. Knee, Quantum leakage detection using a model-independent dimension witness, Phys. Rev. A **99**, 032328 (2019).

[9] J. Helsen, F. Battistel, and B. M. Terhal, Spectral quantum tomography, npj Quantum Inf. **5**, 74 (2019).

[10] J. Zhang and M. Sarovar, Quantum Hamiltonian Identification from Measurement Time Traces, Phys. Rev. Lett. **113**, 080401 (2014).

[11] J. Zhang and M. Sarovar, Identification of open quantum systems from observable time traces, Phys. Rev. A **91**, 052121 (2015).

[12] R. S. Bennink and P. Lougovski, Quantum process identification: A method for characterizing non-Markovian quantum dynamics, New J. Phys. **21**, 083013 (2019).

[13] See Supplemental Material at http://link.aps.org/supplemental/10.1103/PhysRevLett.126.150402 for more details.

[14] V. Scarani, M. Ziman, P. Štelmachovič, N. Gisin, and V. Bužek, Thermalizing Quantum Machines: Dissipation and Entanglement, Phys. Rev. Lett. **88**, 097905 (2002).

[15] M. Ziman and V. Bužek, All (qubit) decoherences: Complete characterization and physical implementation, Phys. Rev. A **72**, 022110 (2005).

[16] A. Sone and P. Cappellaro, Exact dimension estimation of interacting qubit systems assisted by a single quantum probe, Phys. Rev. A **96**, 062334 (2017).

[17] M. Navascués, D. Pérez-García, and I. Villanueva, Testing microscopic discretization, J. Phys. A **46**, 085304 (2013).

[18] Note that the decomposition of the time series into principal components employed here, each of which correspond to rank-1 TD matrices, has close resemblance to the model-free singular spectrum analysis [19].

[19] N. Golyandina, V. Nekrutkin, and A. A. Zhigljavsky, *Analysis of Time Series Structure: SSA and Related Techniques* (CRC Press, Boca Raton, 2001).

[20] S. Ubaru and Y. Saad, Fast methods for estimating the numerical rank of large matrices, in *International Conference on Machine Learning* (Proceedings of Machine Learning Research, New York, 2016), pp. 468–477.

[21] R. Hildner, D. Brinks, J. B. Nieder, R. J. Cogdell, and N. F. van Hulst, Quantum coherent energy transfer over varying pathways in single light-harvesting complexes, Science **340**, 1448 (2013).

[22] E. Thyrhaug, R. Tempelaar, M. J. Alcocer, K. Žídek, D. Bína, J. Knoester, T. L. Jansen, and D. Zigmantas, Identification and characterization of diverse coherences in the fenna–matthews–olson complex, Nat. Chem. **10**, 780 (2018).

[23] G. S. Schlau-Cohen, A. Ishizaki, T. R. Calhoun, N. S. Ginsberg, M. Ballottari, R. Bassi, and G. R. Fleming, Elucidation of the timescales and origins of quantum electronic coherence in lhcii, Nat. Chem. **4**, 389 (2012).

[24] S. Westenhoff, D. Palecek, P. Edlund, P. Smith, and D. Zigmantas, Coherent picosecond exciton dynamics in a photosynthetic reaction center, J. Am. Chem. Soc. **134**, 16484 (2012).

[25] J. Yuen-Zhou, J. J. Krich, I. Kassal, A. S. Johnson, and A. Aspuru-Guzik, *Ultrafast Spectroscopy* (IOP Publishing, Bristol, 2014).

[26] M. Marcus, G. C. Knee, and A. Datta, Towards a spectroscopic protocol for unambiguous detection of quantum coherence in excitonic energy transport, Faraday Discuss. **221**, 110 (2020).

[27] E. Bukartė, A. Haufe, D. Paleček, C. Büchel, and D. Zigmantas, Revealing vibronic coupling in chlorophyll c1 by polarization-controlled 2d electronic spectroscopy, Chem. Phys. **530**, 110643 (2020).

[28] J. Adolphs and T. Renger, How proteins trigger excitation energy transfer in the FMO complex of green sulfur bacteria, Biophys. J. **91**, 2778 (2006).

[29] C. Olbrich, J. Strumpfer, K. Schulten, and U. Kleinekathofer, Theory and simulation of the environmental effects on fmo electronic transitions, J. Phys. Chem. Lett. **2**, 1771 (2011).